Journal of Materials Chemistry A

RSC Publishing

PAPER

View Article Online
View Journal | View Issue

Cite this: J. Mater. Chem. A, 2013, 1, 5840

A hierarchical heterostructure based on Pd nanoparticles/layered double hydroxide nanowalls for enhanced ethanol electrooxidation†

Jingwen Zhao,[a] Mingfei Shao,[a] Dongpeng Yan,[a] Shitong Zhang,[a] Zhenzhi Lu,[a] Zhuoxin Li,[b] Xingzhong Cao,[b] Baoyi Wang,[b] Min Wei,*[a] David G. Evans[a] and Xue Duan[a]

Finely dispersed Pd nanoparticles (PdNPs) anchored to CoAl layered double hydroxide nanowalls (LDH-NWs) have been fabricated *via* a facile *in situ* redox reaction between the LDH-NWs and the $PdCl_4^{2-}$ precursor. The integrated LDH-NWs play the roles of both a hierarchical support and a reductant without any external agent, ensuring the cleanness of the metal–support interface. Based on the effective exposure of the Pd active sites and the elaborate network architecture, the Pd/LDH-NW heterogenous material yields a largely improved catalytic activity as well as robust durability towards ethanol electrooxidation in comparison with the commercial Pd/C catalyst. Moreover, a density functional theory (DFT) calculation indicates that the enhancement in the electrocatalytic properties originates from the synergistic effect between the metal and support, in which the LDH support stabilizes the PdNPs *via* the formation of a Pd–HO bond which is accompanied by an electron transfer from the LDH to the PdNPs. This work provides a promising approach for the design and fabrication of highly efficient metal-supported nanocatalysts which can be used in fuel cells and other related catalytic reactions.

Received 6th February 2013
Accepted 8th March 2013

DOI: 10.1039/c3ta10588a

www.rsc.org/MaterialsA

1 Introduction

Owing to the increasing energy demand from modern manufacture industry, direct alcohol fuel cells (DAFCs) have become the promising energy conversion device for powering portable electronics and on-board vehicles.[1] Direct ethanol fuel cells (DEFCs) are particularly attractive due to their high production, low toxicity and easy manipulation, as well as their high theoretical energy density (8.01 kW h kg^{-1}).[2] Pt-based materials are particularly efficient in this process, but their high cost as well as limited availability restrict their practical applications; moreover, the poisoning of Pt catalysts in alkaline solution also hinders their application in DAFCs.[3] In contrast to traditional Pt catalysts, Pd-based composite catalysts have received considerable attention, with the advantages of a relatively low cost, a high activity and a resistance to poisoning making them excellent candidates for use in DEFCs.[4]

Recently, substantial efforts have been devoted to exploring the Pd-based heteronanostructures with superior performances relative to individual Pd, such as core–shell nanocrystals,[5] bimetallic nanomaterials,[6] conductive carbon-based matrixes (carbon nanotube and graphene, *etc.*) and polymer[7] supported Pd electrocatalysts. In spite of the advanced properties of the hybrid materials, two critical issues remain unresolved. Firstly, for a given loading of noble metal, it is highly desirable for all active sites to be effective in the electrochemical reaction; unfortunately, the disordered architecture limits the penetration/transport of the electrolyte and therefore restricts the effective utilization of the noble metal. Secondly, Pd catalysts prepared by the traditional impregnation route normally suffer from an inferior stability over long-term employment, as a result of the migration/aggregation of the Pd species.[8,9] In addition, it is believed that a strong metal–support interaction plays an important role in controlling the size, dispersion, stability and the resulting catalytic performance.[10] Therefore, the fabrication of sophisticated architectures with highly dispersed Pd nanoparticles (PdNPs) immobilized on a suitable support is of vital importance and remains a challenging goal.

Layered double hydroxides (LDHs) are a class of inorganic lamellar anionic clays consisting of positively charged brucite-like host layers and exchangeable interlayer anions,[11] which have been widely used as promising heterogenerous catalysts and supports.[12] Recently, LDH-based two-dimensional arrays or hierarchical architectures were also reported for developing novel applications.[13] This therefore motivates us to fabricate a

[a]State Key Laboratory of Chemical Resource Engineering, Beijing University of Chemical Technology, Beijing 100029, China. E-mail: weimin@mail.buct.edu.cn; Fax: +86-10-64425385; Tel: +86-10-64412131

[b]Institute of High Energy Physics, Chinese Academy of Sciences, Beijing 100049, China

† Electronic supplementary information (ESI) available. See DOI: 10.1039/c3ta10588a

well-ordered LDH hierarchical network which can act as both a support and a reductant for the *in situ* anchoring of PdNPs, so as to improve the electrocatalytic behavior. The resulting Pd-based electrocatalyst would offer the following advantages: (i) the LDH matrix would provide a confined and stable microenvironment for the *in situ* formation of PdNPs with a uniform particle size and high dispersion, owing to the ordered arrangement of the cationic reductant in the LDH layers; (ii) the resulting PdNP/LDH heterostructure endows specific metal–support interactions at the interface which would facilitate the reactivity of the PdNPs; (iii) the PdNP/LDH hierarchical network would further improve the mass/electron transport during the electrocatalytic reaction.

Herein, we demonstrate the design and fabrication of a hierarchical Pd-based heteronanostructure with finely dispersed PdNPs anchored to the vertically aligned LDH-NWs by using an *in situ* spontaneous deposition route. The loading of the PdNPs is amazingly triggered by a direct redox reaction between the Co^{2+} species within the LDH-NWs and the $PdCl_4^{2-}$ in solution, in which the LDH-NWs serve as both a reductant and a size-controlling support (shown in Scheme 1). Owing to the effective exposure of the Pd active sites and the elaborate network architecture, the as-prepared Pd/LDH-NW catalyst yields a largely improved catalytic activity as well as robust durability towards ethanol electrooxidation in comparison with the commercial Pd/C catalyst. DFT calculations further reveal that the enhancement in the electrocatalytic properties originates from a strong synergistic effect between the metal and support, in which a direct Pd–HO interaction accompanied by a facile electron transfer occurs at the metal–support interface. The control over the reactivity and stability of the supported PdNPs demonstrated in this work offers a promising strategy for the fabrication of metal nanocatalysts for highly efficient DEFCs.

2 Experimental details

2.1 Synthesis of the LDH-NWs and the Pd/LDH-NWs

The sample of LDH-NWs was prepared using a solvothermal direct growth process on ITO substrates. $Co(NO_3)_2 \cdot 6H_2O$ (1 mmol), $Al(NO_3)_3 \cdot 9H_2O$ (0.5 mmol), NH_4F (5 mmol) and urea (35 mmol) were dissolved in 50 mL of deionized water with $n(Co) : n(Al) = 2 : 1$. The homogeneous solution was stirred thoroughly for 30 min. The ITO substrates were cleaned in an ultrasonic bath containing soapy water, deionized water, acetone, ethanol and deionized water for 10 min each. Subsequently, a piece of ITO substrate was immersed into the aqueous solution at 95 °C for 6 h. The substrate coated with LDH-NWs was then withdrawn from the solution, washed extensively with distilled water and dried at room temperature.

The synthesis of Pd/LDH-NWs was carried out by simply soaking the above LDH-NWs in a K_2PdCl_4 aqueous solution at different temperatures for 10 min, so as to allow the immobilization of PdNPs based on the redox reaction between Co^{2+} in LDH-NWs and $PdCl_4^{2-}$. Finally, the resulting Pd/LDH-NWs was washed thoroughly with water to remove the remaining reagents and dried at ambient temperature.

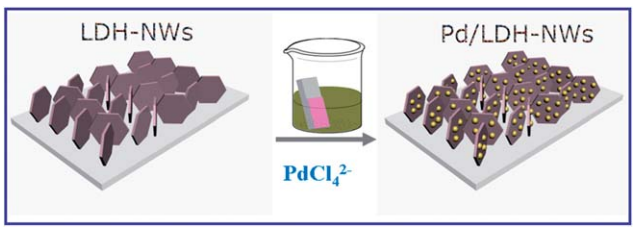

Scheme 1 A schematic representation for the Pd/LDH-NW heteronanostructure with highly dispersed PdNPs.

2.2 Material characterization

X-ray diffraction (XRD) patterns were recorded using a Rigaku XRD-6000 diffractometer, using Cu-Kα radiation (0.15418 nm) at 40 kV, 30 mA. The morphology was investigated using a scanning electron microscope (SEM; Zeiss SUPRA 55) with an accelerating voltage of 20 kV, combined with energy dispersive X-ray spectroscopy (EDX). Transmission electron microscopy (TEM) images were recorded using a Philips Tecnai 20 and a JEOL JEM-2010 HR-TEM. X-ray photoelectron spectroscopy (XPS) measurements were performed using an ESCALAB 250 instrument (Thermo Electron) with Al-Kα radiation. Fourier transform infrared (FT-IR) spectra were obtained using a Vector 22 (Bruker) spectrophotometer with 2 cm^{-1} resolution. Positron annihilation experiments were carried out using a fast–slow coincidence ORTEC system with a time resolution of 197 ps full width at half maximum. A 1.1×10^6 Bq source of ^{22}Na was sandwiched between two identical samples. The positron annihilation results were analyzed using the LT-9 program. A CHI 660B electrochemical workstation (Shanghai Chenhua Instrument Co., China) was utilized for the electrochemical measurements. A conventional three-electrode cell was used with a saturated Hg/HgO electrode as the reference, a platinum wire as the counter, and the modified ITO electrode as the working electrode. Electrocatalytic oxidation of ethanol was measured in a mixture of 0.05 M ethanol and 1 M NaOH. A commercial 10 wt% Pd/C catalyst (Aldrich Chem Co. Ltd) and a Pd-supported CoAl-LDH powdered sample were used as comparison materials. Electrochemical impedance spectroscopy (EIS) dispersions were recorded in the frequency range 0.01–100 kHz in a 0.1 M KNO_3 with 1 mM $Fe(CN)_6^{4-/3-}$ solution.

3 Results and discussion

Fig. 1A displays a typical photograph of the large-scale CoAl-LDH nanowalls (LDH-NWs) obtained *via* a solvothermal direct growth process on an ITO substrate (see the ESI†). The low-magnification SEM image of the as-prepared LDH-NWs (Fig. 1B) shows a high density and uniform coating covering the entire substrate surface; the magnified image (Fig. 1C) displays an integrated nanowall network in which the LDH microcrystals stand perpendicularly on the ITO substrate and intercross with each other. X-ray energy dispersive spectroscopy (EDS) (inset of

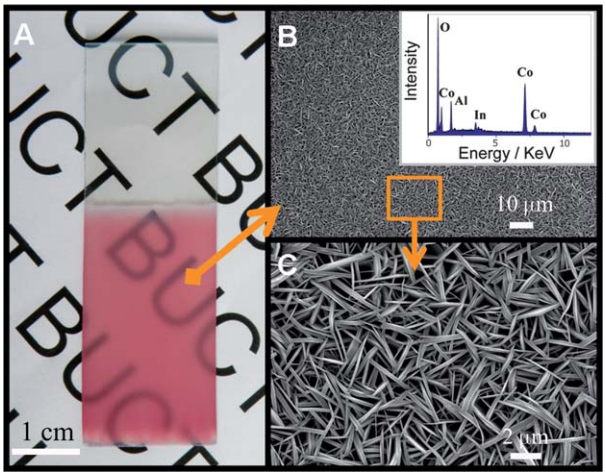

Fig. 1 (A) A digital photograph of large-scale LDH-NWs grown on an ITO substrate. SEM images of the LDH-NWs at (B) low magnification (inset: the corresponding EDS results) and (C) high magnification.

Fig. 1B) demonstrates the existence of cobalt, aluminum and oxygen in the nanowalls with a Co : Al molar ratio of 1.97, which is in line with the nominal ratio (Co : Al = 2 : 1).

The XRD pattern of the CoAl-LDH powdered sample scraped from the ITO substrate (Fig. 2A, curve b) can be indexed to a rhombohedral LDH phase with the refined lattice parameters of $a = 3.0693$ Å and $c = 22.838$ Å (Joint Committee on Powder Diffraction Standards (JCPDS) file no. 51-0045). In contrast to the scraped sample with a random orientation of LDH crystallites, the XRD pattern of the LDH-NWs on the substrate (Fig. 2A, curve a) only displays four clear reflections that correspond to the [012], [015], [110] and [113] planes; the absence of (00*l*) reflections indicates the preferential orientation of the LDH crystallites, with the *ab*-plane perpendicular to the substrate.[14] The representative cross-sectional morphology of the LDH-NWs (Fig. 2B) combined with the EDS line scan (Fig. S1†) demonstrates a monolayer of LDH crystals with an average lateral size of ~1.5 μm vertically aligned on the substrate, which confirms the heteronucleation of CoAl-LDH on the ITO surface (see FT-IR spectrum, Fig. S2†). The TEM image (Fig. 2C) displays a hexagonal morphology of a single CoAl-LDH nanocrystal with a particle size of ~1.5 μm, which approximately agrees with that of the SEM image (Fig. 2B). The corresponding selected area electron diffraction (SAED) pattern (Fig. 2D) exhibits hexagonally arranged spots, indicating the high crystallinity of the LDH-NWs; the hexagonal lattice with $a = 3.07$ Å is consistent with the in-plane structural parameter determined from the original XRD pattern (Fig. 2A).

In a typical synthesis of the Pd/LDH-NW heternanostructure, the LDH-NW sample was simply immersed into a K_2PdCl_4 aqueous solution at room temperature for 10 min without stirring. TEM images (Fig. 3A and B) reveal that the PdNPs are well monodispersed on the surface of the LDH nanocrystal with a uniform particle size of ~1.8 nm. The EDS analysis also confirms the introduction of Pd onto the LDH-NWs (inset of Fig. 3A), and the XRD measurement indicates that the deposition process occurred on the surface of the LDH without the use of an interlayer gallery (Fig. S3†). As can be seen from the HRTEM image (Fig. 3C), the lattice fringes of 0.227 and 0.197 nm agree well with the (111) and (200) lattice spacing of the face centered cubic (fcc) Pd crystal. The crystalline structure of the PdNPs was further verified by the fast Fourier transformation (FFT) of the HRTEM image (Fig. 3D), in which two main diffraction rings corresponding to the (111) and (200) plane lattice of Pd were observed. Moreover, the hexagonal diffraction in the FFT pattern is attributed to the {1010} crystalline planes of the LDH phase, suggesting that the support structure is maintained upon the immobilization of the PdNPs.

The surface characterization of the Pd/LDH-NW was further studied by X-ray photoelectron spectroscopy (XPS). Fig. 4A (curve b) shows the XPS spectrum of the Pd (3d) envelope, in

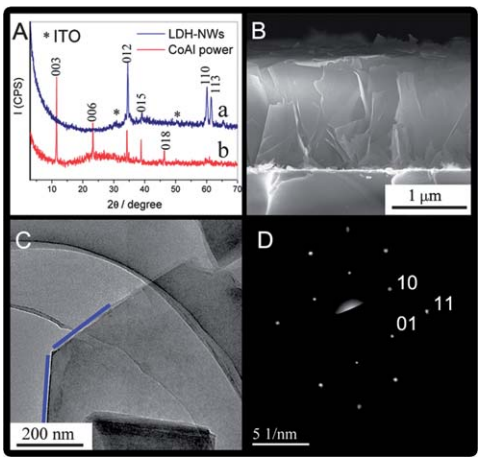

Fig. 2 (A) XRD patterns of (a) the as-prepared LDH-NWs and (b) the powdered material scraped from the film. The symbol "*" indicates the reflections from the ITO substrate. (B) A typical cross-sectional SEM image of the LDH-NWs. (C) A TEM image of a single CoAl-LDH nanocrystal grown on the ITO substrate and (D) the corresponding selected area electron diffraction (SAED) pattern.

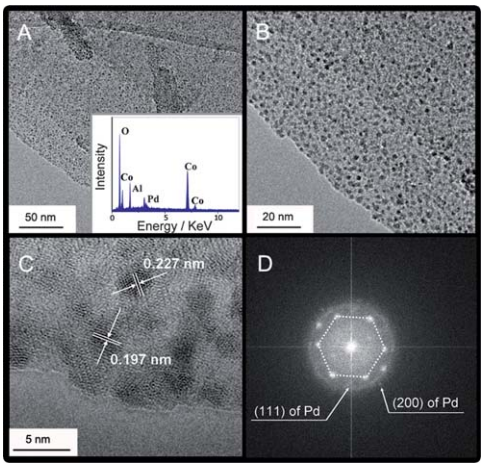

Fig. 3 TEM images of the as-prepared Pd/LDH-NW at (A) low magnification (inset: the corresponding EDS analysis) and (B) high magnification. (C) The HRTEM image of the Pd/LDH-NW and (D) the corresponding fast Fourier transformation (FFT) pattern.

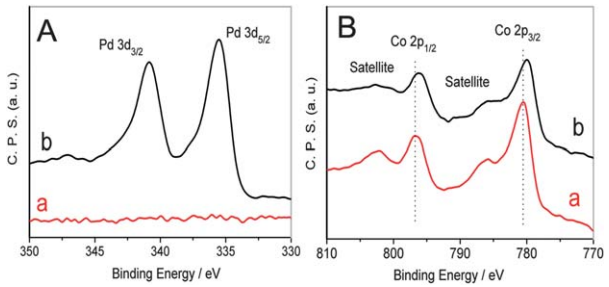

Fig. 4 The XPS spectra of (A) Pd 3d and (B) Co 2p: (a) LDH-NWs and (b) Pd/LDH-NWs.

which the binding energies of 335.4 and 341.2 eV corresponding to the $3d_{5/2}$ and $3d_{3/2}$ of the metallic Pd(0) state were observed respectively, indicating the presence of metallic Pd.[15] The Co 2p core lines of the pristine LDH-NW support are split into Co $2p_{3/2}$ (780.5 eV) and Co $2p_{1/2}$ (796.7 eV) peaks and are accompanied by satellite bands at 785.5 and 802.1 eV (Fig. 4B, curve a), which are indicative of a high-spin Co^{2+} state in the LDH-NW support.[16] After the *in situ* deposition of the PdNPs, both the Co $2p_{3/2}$ and Co $2p_{1/2}$ peaks shift to lower energy levels (779.9 and 796.2 eV, respectively), and there is a slight decrease in the intensity of the satellite bands (Fig. 4B, curve b). Such observations indicate the occurrence of a partial valence change from Co^{2+} to Co^{3+},[17] implying that the driving force for the immobilization of the PdNPs arises from the redox reaction between $PdCl_4^{2-}$ in solution and Co^{2+} in the LDH support. To further prove this point, a comparison study was carried out by soaking a MgAl-LDH sample in a K_2PdCl_4 aqueous solution under the same conditions. Two peaks at 337.2 and 342.4 eV attributed to the $3d_{5/2}$ and $3d_{3/2}$ of Pd(II) were observed (Fig. S4†, curve a),[18] suggesting a simple adsorption of $PdCl_4^{2-}$ onto the surface of MgAl-LDH without any redox process. Therefore, it is reasonable to propose that the redox reaction between CoAl-LDH and $PdCl_4^{2-}$ accounts for the *in situ* spontaneous deposition of the PdNPs onto the LDH surface, which is similar to the reaction mechanism between iodine and CoFe-LDH reported by Sasaki *et al.*[17a] Interestingly, the size of the PdNPs can be easily tuned *via* simply changing the deposition temperature (Fig. S5†), and the sample obtained at 25 °C shows the highest electrocatalytic activity (Fig. S6†). In this work, the integrated LDH-NWs play the roles of both a support and a reductant without any external agent, guaranteeing the cleanness of the metal–support interface without impurities. In addition, the specific ordered arrangement of the di- and tri-valent cations in the LDH phase provides dispersive and uniform Co^{2+} active sites for the reduction of $PdCl_4^{2-}$, imparting a good microenvironment for the nucleation and stabilization of the PdNPs. Therefore, the spontaneous deposition strategy in this work affords clean and well-dispersed PdNPs anchored to the LDH-NWs.

The catalytic activity of the Pd/LDH-NW towards ethanol electrooxidation was evaluated in an alkaline medium with a commercial Pd/C catalyst and a Pd-supported LDH powdered material (Pd/LDH) as comparison samples. The cyclic voltammograms (CVs) of the three catalysts recorded in 1.0 M NaOH without ethanol are shown in Fig. 5A. Since hydrogen can penetrate into the Pd lattices, the electrochemically active surface areas (ECSAs) were calculated by measuring the charge collected in the reduction region of PdO/Pd at ~−0.2 V with the double-layer correction, assuming 0.405 mC cm^{-2} for the reduction of a monolayer PdO on the catalyst surface.[19] The oxidation currents were normalized to the ECSAs (1.147 cm^2 for Pd/LDH-NWs, 0.739 cm^2 for Pd/C and 0.668 cm^2 for Pd/LDH) for further comparison. In the presence of 1.0 M NaOH and 0.05 M ethanol, the Pd/LDH-NW catalyst exhibits the highest electrocatalytic activity with a forward oxidation current density (j_F) and a reverse oxidation current density (j_R) of 2.01 and 2.20 mA cm^{-2}, respectively, which is much larger than those of the Pd/C (0.41 and 0.34 mA cm^{-2}) and the Pd/LDH (0.51 and 0.55 mA cm^{-2}) (Fig. 5B). Moreover, both the peak and onset potentials are noticeably more negative on the Pd/LDH-NWs than on the Pd/C and Pd/LDH, indicating a significant enhancement in the kinetics of the ethanol electrooxidation reaction.[20]

The improved electrocatalytic performance is further demonstrated by its enhanced long-term durability. Chronoamperometric curves recorded at −0.3 V for 2200 s are illustrated in Fig. 5C. The initial rapid decrease in the polarization current for all the samples is attributed to the poisoning effect of the intermediate species during the ethanol electrooxidation reaction in alkaline media. Subsequently, the current decreases slowly and reaches a pseudosteady state.[7e,20b] The current densities on the Pd/LDH-NWs are significantly higher than those on the Pd/C and Pd/LDH over the entire time range. After 500 potential cycles, 96.0% and 87.6% of the initial catalytic activities in the positive- and negative-going potential scans were still maintained for the Pd/LDH-NWs (Fig. 5D and Table S1†), which is highly superior to the Pd/C and Pd/LDH samples (Table S2†).

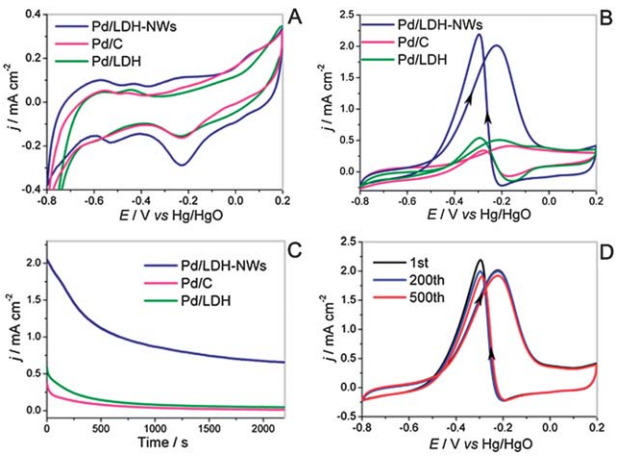

Fig. 5 Cyclic voltammograms of the Pd/LDH-NW, Pd/C and Pd/LDH at 50 mV s^{-1} in (A) 1 M NaOH and (B) 1 M NaOH + 0.05 M ethanol. Electrocatalytic stability test: (C) chronoamperometric curves for ethanol electrooxidation at −0.3 V *vs* Hg/HgO on the Pd/LDH-NW, Pd/C and Pd/LDH in 1 M NaOH + 0.05 M ethanol; (D) cyclic voltammograms (1st, 200th and 500th cycle) of the Pd/LDH-NW sample for ethanol electrooxidation at 50 mV s^{-1}.

In alkaline media, the widely accepted mechanism of ethanol oxidation on the surface of a Pd electrode can be expressed by the following equations:

$$CH_3CH_2OH + 3OH^- \rightarrow CH_3CO_{ads} + 3H_2O + 3e^- \quad (1)$$

$$CH_3CO_{ads} + OH^-_{ads} \rightarrow CH_3COOH \quad (2)$$

$$CH_3COOH + OH^- \rightarrow CH_3COO^- + H_2O \quad (3)$$

since breaking the C–C bond for a total oxidation to CO_2 suffers from a much higher energy barrier compared with other steps, acetate salt might be the final product.[3d,4e,20b] The rate-determining step is the removal of the adsorbed ethoxy (CH_3CO_{ads}) by the adsorbed hydroxyl (OH^-_{ads}).[3d] It has been reported that OH^-_{ads} is readily produced on the surface of metal oxides, which leads to the decrease in the barrier energy of the CH_3CO_{ads} oxidization.[4d,20c] In this regard, adequate OH^-_{ads} species supplied by the LDH support can significantly accelerate the rate-determining step, as evidenced by the negative-shift in the peak potential as well as the enhanced current density (Fig. 5B).

Electrochemical impedance spectra (EIS) were also performed to demonstrate the merits of the Pd/LDH-NWs arising from their vertically aligned configuration (Fig. S7A†, with an equivalent circuit shown in Fig. S7B†). The Nyquist plot of the powdered Pd/LDH sample exhibits only one semicircle, which corresponds to the charge-transfer process at the LDH/Pd–electrolyte interface. In the case of the Pd/LDH-NWs, two semicircles were observed in the Nyquist plot. The large one in the low frequency region is due to the charge-transfer occurring at the LDH/Pd–electrolyte interface while the small one is associated with the resistance of the ITO–electrolyte interface.[21] This result indicates that the hierarchical network of the Pd/LDH-NWs facilitates the penetration of the electrolyte to the bottom of the nanowalls and thus enhances the accessibility of the channels for the electrolyte, which guarantees a high energy density during the electrooxidation. Moreover, N_2 gas adsorption–desorption measurements on the Pd/LDH-NWs (Fig. S8†) reveal that the sample displays type IV isotherms with H3 type hysteresis loops, with a mesopore distribution in the size range 2–5 nm, which benefits the mass/charge diffusion in a solid.[22] Owing to the hierarchically mesoporous architecture and the highly dispersed PdNPs, the Pd/LDH-NW electrode possesses a remarkable catalytic activity as well as a superior stability in the electrooxidation reaction.

To gain a further insight into the intrinsic activity for the present electrocatalyst, a DFT calculation was conducted to elucidate the metal–support interactions for the Pd/LDH heterostructure from a theoretical viewpoint. A Pd_9 cluster is used to represent the Pd(111) surface which dominates the Pd-based catalyst with a fcc structure as discussed above. The structural model of the Pd_9 cluster supported on the CoAl-LDH (Co : Al = 2 : 1) is shown in Fig. 6A. The metal cluster directly interacts with the LDH layer *via* four Pd atoms, giving a binding energy of −5.829 eV with respect to the pristine LDH and Pd_9 species. The hydroxy protons were found to point towards the Pd atoms with the H–Pd distance in the range of 1.895–2.547 Å at the interface, and the O–H bonds were significantly elongated by 0.03–0.07 Å

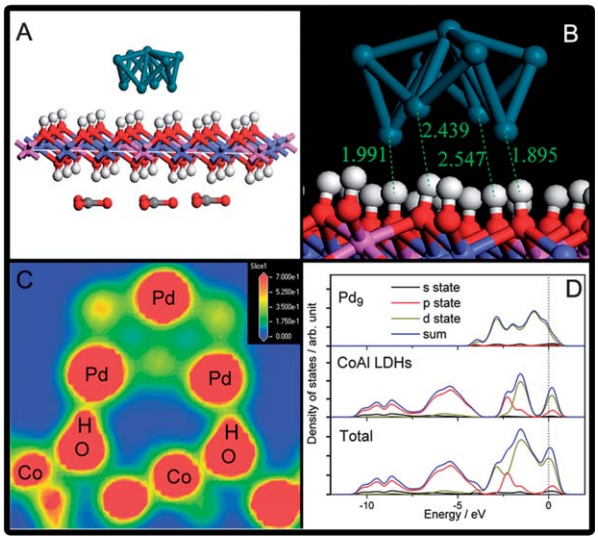

Fig. 6 (A) The structural model of Pd_9/CoAl-LDH (white, H; pink, Al; red, O; blue, Co; dark cyan, Pd). (B) The optimized Pd_9/CoAl-LDH interface with the corresponding Pd–H distance (Å). (C) The electron density contour map of Pd_9/CoAl-LDH, with the electron density range of 0.0–0.7 e $Å^{-3}$. (D) The total and local density of states (TDOS and LDOS) for the Pd_9/CoAl-LDH system, with the Fermi level (black dashed line) as the reference of zero energy.

compared with those in the pristine LDH (Fig. 6B). The results indicate that the surface hydroxyls of the LDH play an essential role in stabilizing the Pd clusters through an effective Pd–HO interaction. This stabilization can be further demonstrated by the local density of states (LDOS) for Pd, in which the gravity center of the d-band shifts to a lower energy with respect to the Fermi level for the Pd_9/CoAl-LDH system compared with the pristine Pd_9 cluster (Fig. S9†).

Further Mulliken population analysis shows that the Pd_9 cluster contains a negative charge with −0.11 e per atom by electron transfer from the LDH. The partial superimposition of the electron densities between the metal and support confirms the charge perturbation (Fig. 6C), indicating that the agostic bond-like interaction at the interface involves the Pd–HO bond with a metallic/covalent nature where electrons are shared. Moreover, the palladium states essentially fill the whole band gap and contribute to the HOMO–LUMO region (Fig. 6D), suggesting that the electrons from Pd_9 are delocalized and extensively overlap with the support. Positron annihilation spectrometry, which is a well-established technique to convey information on the local electronic environment in materials,[23] was carried out in this work. The positron lifetime spectra in the present case (Table S3†) provide further evidence for the prior trapping and positrons annihilation occurring near the PdNPs with an enhanced electron density, which corresponds to the remarkable electron transfer in the Pd/LDH system (see ESI† for more details). The redistribution of charge density in the metal clusters is expected to be crucial for the catalytic reactivity of molecular adsorbates on supports.[24] The negatively charged PdNPs strengthen the back donation of electron density into the antibonding orbitals of ethanol molecule or intermediates, so as to reduce the dissociation barrier and facilitate the bond

cleavage, accounting for the extraordinarily high catalytic activity of the Pd/CoAl-LDH system.

4 Conclusions

In conclusion, a facile and cost-effective strategy has been developed to anchor PdNPs onto the hierarchical LDH-NW support for highly efficient ethanol electrooxidation. Based on an *in situ* redox reaction between the LDH-NW support and metal salt precursor, a well-designed Pd/LDH-NW heteronanostructure with a mesoporous architecture as well as a uniform dispersion of anchored PdNPs was obtained, which exhibits excellent catalytic activity and robust durability for ethanol electrooxidation. A combined DFT calculation and positron annihilation study indicates that the LDH support stabilizes the PdNPs *via* the formation of a Pd–HO bond, and the redistribution of charge density (electron transfer from LDH to PdNPs) further facilitates the process of ethanol electrooxidation. It is anticipated that the facile approach can be extended to the fabrication of other immobilized metal nanocatalysts within a hierarchical support for potential applications in fuel cells and heterogeneous catalysis.

Acknowledgements

This work was supported by the 973 Program (Grant no.: 2011CBA00504), the National Natural Science Foundation of China (NSFC) and the Beijing Natural Science Foundation (2132043). M. Wei particularly appreciates the financial aid from the China National Funds for Distinguished Young Scientists of the NSFC.

Notes and references

1 (*a*) C. Lamy, E. M. Belgsir and J.-M. Léger, *J. Appl. Electrochem.*, 2001, **39**, 799; (*b*) B. C. H. Steele and A. Heinzel, *Nature*, 2001, **414**, 345; (*c*) Z. Xia, S. Wang, Y. Li, L. Jiang, H. Sun, S. Zhu, D. S. Su and G. Sun, *J. Mater. Chem. A*, 2013, **1**, 491.

2 (*a*) C. Bianchini and P. K. Shen, *Chem. Rev.*, 2009, **109**, 4183; (*b*) L. An and T. S. Zhao, *Energy Environ. Sci.*, 2011, **4**, 2213; (*c*) J. R. Varcoe and R. C. T. Slade, *Fuel Cells*, 2005, **5**, 187.

3 (*a*) C. Koenigsmann and S. S. Wong, *Energy Environ. Sci.*, 2011, **4**, 1161; (*b*) E. Antolini, *J. Power Sources*, 2007, **170**, 1; (*c*) G. Yang, Y. Li, R. K. Rana and J. J. Zhu, *J. Mater. Chem. A*, 2013, **1**, 1754; (*d*) W. Du, K. E. Mackenzie, D. F. Milano, N. A. Deskins, D. Su and X. Teng, *ACS Catal.*, 2012, **2**, 287.

4 (*a*) E. Antolini, *Energy Environ. Sci.*, 2009, **2**, 915; (*b*) C. Xu, L. Cheng, P. Shen and Y. Liu, *Electrochem. Commun.*, 2007, **9**, 997; (*c*) Z. Cui, C. Gong, C. X. Guo and C. M. Li, *J. Mater. Chem. A*, 2013, **1**, 1179; (*d*) E. D. Wang, J. B. Xu and T. S. Zhao, *J. Phys. Chem. C*, 2010, **114**, 10489; (*e*) G. Cui, S. Song, P. K. Shen, A. Kowal and C. Bianchini, *J. Phys. Chem. C*, 2009, **113**, 15639.

5 (*a*) C.-L. Lu, K. S. Prasad, H.-L. Wu, J.-A. Ho and M. H. Huang, *J. Am. Chem. Soc.*, 2010, **132**, 14546; (*b*) D. Kim, Y. W. Lee, S. B. Lee and S. W. Han, *Angew. Chem., Int. Ed.*, 2012, **51**, 159.

6 (*a*) S. Shen and T. Zhao, *J. Mater. Chem. A*, 2013, **1**, 906; (*b*) F. Ksar, L. Ramos, B. Keita, L. Nadjo, P. Beaunier and H. Remita, *Chem. Mater.*, 2009, **21**, 3677; (*c*) F. Lan, D. Wang, S. Lu, J. Zhang, D. Liang, S. Peng, Y. Liu and Y. Xiang, *J. Mater. Chem. A*, 2013, **1**, 1548.

7 (*a*) S. Sattayasamitsathit, Y. Gu, K. Kaufmann, W. Jia, X. Xiao, M. Rodriguez, S. Minteer, J. Cha, D. B. Burckel, C. Wang, R. Polsky and J. Wang, *J. Mater. Chem. A*, 2013, **1**, 1639; (*b*) B. J. Gallon, R. W. Kojima, R. B. Kaner and P. L. Diaconescu, *Angew. Chem., Int. Ed.*, 2007, **46**, 7251; (*c*) D. Wang, S. Lu, P. J. Kulesza, C. M. Li, R. D. Marco and S. P. Jiang, *Phys. Chem. Chem. Phys.*, 2011, **13**, 4400; (*d*) M. Sawangphruk, A. Krittayavathananon and N. Chinwipas, *J. Mater. Chem. A*, 2013, **1**, 1030; (*e*) Z.-Y. Zhou, Z.-Z. Huang, D.-J. Chen, Q. Wang, N. Tian and S.-G. Sun, *Angew. Chem., Int. Ed.*, 2010, **49**, 411.

8 (*a*) K. K. R. Datta, B. V. S. Reddy, K. Ariga and A. Vinu, *Angew. Chem., Int. Ed.*, 2010, **49**, 5961; (*b*) L. Chen, J. Hu and R. Richards, *J. Am. Chem. Soc.*, 2009, **131**, 914.

9 (*a*) A. J. Amali and R. K. Rana, *Chem. Commun.*, 2008, 4165; (*b*) B. Yoon and C. M. Wai, *J. Am. Chem. Soc.*, 2005, **127**, 17174; (*c*) M.-Q. Zhao, Q. Zhang, W. Zhang, J.-Q. Huang, Y. Zhang, D. S. Su and F. Wei, *J. Am. Chem. Soc.*, 2010, **132**, 14739.

10 (*a*) G. N. Vayssilov, Y. Lykhach, A. Migani, T. Staudt, G. P. Petrova, N. Tsud, T. Skála, A. Bruix, F. Illas, K. C. Prince, V. Matolín, K. M. Neyman and J. Libuda, *Nat. Mater.*, 2011, **10**, 310; (*b*) J. R. B. Gomes, Z. Lodziana and F. Illas, *J. Phys. Chem. B*, 2003, **107**, 6411.

11 (*a*) P. J. Sideris, U. G. Nielsen, Z. Gan and C. P. Grey, *Science*, 2008, **321**, 113; (*b*) A. M. Fogg, V. M. Green, H. G. Harvey and D. O'Hare, *Adv. Mater.*, 1999, **11**, 1466; (*c*) R. Ma, K. Takada, K. Fukuda, N. Iyi, Y. Bando and T. Sasaki, *Angew. Chem., Int. Ed.*, 2008, **47**, 86; (*d*) L. F. S. da Silva, G. J.-F. Demets, C. Taviot-Guého, F. Leroux and J. B. Valim, *Chem. Mater.*, 2011, **23**, 1350.

12 (*a*) J. J. Woodford, J.-P. Dacquin, K. Wilson and A. F. Lee, *Energy Environ. Sci.*, 2012, **5**, 6145; (*b*) J. S. Valente and R. Quintana-Solorzano, *Energy Environ. Sci.*, 2011, **4**, 4096; (*c*) A. Noujima, T. Mitsudome, T. Mizugaki, K. Jitsukawa and K. Kaneda, *Angew. Chem., Int. Ed.*, 2011, **50**, 2986; (*d*) L. Teruel, Y. Bouizi, P. Atienzar, V. Fornes and H. Garcia, *Energy Environ. Sci.*, 2010, **3**, 154; (*e*) L. Li, R. Ma, Y. Ebina, K. Fukuda and T. Sasaki, *J. Am. Chem. Soc.*, 2007, **129**, 8000; (*f*) B. M. Choudary, S. M. Madhi, N. S. Chowdari, M. L. Kantam and B. Sreedhar, *J. Am. Chem. Soc.*, 2002, **124**, 14127.

13 (*a*) K. Mandel, A. D. Tuhtan, F. Hutter, C. Gellermann, H. Steinmetz and G. Sextl, *J. Mater. Chem. A*, 2013, **1**, 1840; (*b*) Z.-L. Hsieh, M.-C. Lin and J.-Y. Uan, *J. Mater. Chem.*, 2011, **21**, 1880; (*c*) J. Liu, Y. Li, X. Huang, G. Li and Z. Li, *Adv. Funct. Mater.*, 2008, **18**, 1448; (*d*) M. Shao, F. Ning, J. Zhao, M. Wei, D. G. Evans and X. Duan, *J. Am. Chem. Soc.*, 2012, **134**, 1071; (*e*) J. Yuan, C. Yu, X. Fan, Z. Ling, J. Qiu and Y. Gogotsi, *J. Mater. Chem. A*, 2013, **1**, 1963.

14 H. Chen, F. Zhang, S. Fu and X. Duan, *Adv. Mater.*, 2006, **18**, 3089.

15 (*a*) H. Meng, C. Wang, P. K. Shen and G. Wu, *Energy Environ. Sci.*, 2011, **4**, 1522; (*b*) Y. E. Cheon and M. P. Suh, *Angew. Chem., Int. Ed.*, 2009, **48**, 2899.

16 (*a*) Q. Tang, Q. Zhang, P. Wang, Y. Wang and H. Wan, *Chem. Mater.*, 2004, **16**, 1967; (*b*) T. J. Chuang, C. R. Brundle and D. W. Rice, *Surf. Sci.*, 1976, **59**, 413.

17 (*a*) R. Ma, J. Liang, K. Takada and T. Sasaki, *J. Am. Chem. Soc.*, 2011, **133**, 613; (*b*) R. Xu and H. C. Zeng, *Chem. Mater.*, 2001, **13**, 297.

18 (*a*) Q. Ye, X. Wang, H. Hu, D. Wang, S. Li and F. Zhou, *J. Phys. Chem. C*, 2009, **113**, 7677; (*b*) D. Ishii, T. Nagashima, M. Udatsu, R.-D. Sun, Y. Ishikawa, S. Kawasaki, M. Yamada, T. Iyoda and M. Nakagawa, *Chem. Mater.*, 2006, **18**, 2152.

19 (*a*) L. Jiang, A. Hsu, D. Chu and R. Chen, *J. Electrochem. Soc.*, 2009, **156**, B370; (*b*) Z. Zhang, K. L. More, K. Sun, Z. Wu and W. Li, *Chem. Mater.*, 2011, **23**, 1570.

20 (*a*) L. Wang, Y. Nemoto and Y. Yamauchi, *J. Am. Chem. Soc.*, 2011, **133**, 9674; (*b*) C. Xu, H. Wang, P. K. Shen and S. P. Jiang, *Adv. Mater.*, 2007, **19**, 4256; (*c*) C. Xu, P. K. Shen and Y. Liu, *J. Power Sources*, 2007, **164**, 527.

21 (*a*) F. Fabregat-Santiago, G. Garcia-Belmonte, J. Bisquert, A. Zaban and P. Salvador, *J. Phys. Chem. B*, 2002, **106**, 334; (*b*) J. Qu, X. P. Gao, G. R. Li, Q. W. Jiang and T. Y. Yan, *J. Phys. Chem. C*, 2009, **113**, 3359.

22 N. Leventis, S. Mulik, X. Wang, A. Dass, C. Sotiriou-Leventis and H. Lu, *J. Am. Chem. Soc.*, 2007, **129**, 10660.

23 (*a*) Q. Xu, T. Yoshiie and K. Sato, *Philos. Mag. Lett.*, 2008, **88**, 353; (*b*) J. Xu, A. P. Mills Jr, A. Ueda, D. O. Henderson, R. Suzuki and S. Ishibashi, *Phys. Rev. Lett.*, 1999, **83**, 4586; (*c*) N. Taguchi, F. Hori, T. Iwai, A. Iwase, T. Akita and S. Tanaka, *Appl. Surf. Sci.*, 2008, **255**, 164.

24 G. N. Vayssilov, B. C. Gates and N. Rösch, *Angew. Chem., Int. Ed.*, 2003, **42**, 1391.

